Influence of Mg^{2+}substitution on particle size distribution for nanocrystalline spinel ferrite system $Mg_xMn_{1-x}Fe_2O_4$ (x = 0.0 – 0.5)

T. K. PATHAK[1,*], K. G. VYAS[2], P. K. RATHOD[3], D. D. PANDYA[1], H. M. MAKADIA[1], S. G. SONCHHATRA[1], K. M. KOROT[4]
[1]*Government Engineering College, Rajkot 360 005, India*
[2]*Department of Physics, Saurashtra University, Rajkot 360 005, Gujarat, India*
[3]*Gujarat Technological University, Ahmedabad, 382 424, Gujarat, India*
[4]*Department of Science and Humanities, Government Engineering College – Palanpur, 385 001, Affiliated to Gujarat Technological University, Ahmedabad, Gujarat, India*

Spinel ferrite system with chemical formula $Mg_xMn_{1-x}Fe_2O_4$ (x = 0.0 – 0.5) having nanoparticle size (25 – 40 nm) were prepared by coprecipitation technique. X – ray diffraction patterns show single phase of the material, EDAX study shows stoichiometry of the samples, whereas particle morphology was studied by means of Transmission electron microscopic analysis (TEM), particles are found to have spherical in nature. In our previous communications we have reported the effect of Mg^{2+} substitution in change of particle shape from spherical to needle shape and on the magnetic properties. In the present work we have studied influence of Mg^{2+} substitution on particle size distribution with the help of differential size distribution (DSD) and Cumulative undersize distribution (CUSD) curves for two representatives amples x = 0.2 and 0.4 for the system $Mg_xMn_{1-x}Fe_2O_4$.

(Received July 30, 2025; accepted February 4, 2026)

Keywords: Nanomaterials, Spinel ferrites, Mg^{2+}, Coprecipitation technique, Particle size distribution

1. Introduction

Ferrites are studied very well by many researchers over the past 50 years [1]. In the field of nanoscience ferrites plays a key role due to its technological applications [2,3]. Mixed transition metal oxides (MTMO) are ideal materials for sensors, solar cells, photocatalysis and supercapacitor electrodes [1]. MTMO which are ternary metal oxides with two different metal cations have gotten lots of attention in recent years because of their variety of applications [1-3]. Among the different spinel ferrites $MnFe_2O_4$ is very interesting one because when Mn – ion occupies the tetrahedral position, its oxidation state changes from 3+ to 2+ and the change compositional phenomenon creates Mn^{4+}. The coexistence of Mn^{2+}, Mn^{3+} and Mn^{4+} in this material creates oxygen vacancies which favors the occurrence of relaxation mechanism [4]. On the other hand, Mg – based nano ferrites are extensively used in biomedical applications [4]. Furthermore, $MgFe_2O_4$ are utilized in a broad category of applications like catalysis, sensors, magnetic technologies etc. [4-6].

Size of particles influences many properties of particulate material. Furthermore, it is a valuable indicator of quality and performance of material. In many applications, particle size plays critical role. For example, it determines (a) appearance and gloss of paint (b) flavor of coco powder (c) reflectivity of highway paint (d) absorption rate of pharmaceuticals (e) appearance of cosmetics and (f) hydration rate and strength of cement. Of course, this is more applicable to nano regime. Particle size distribution data can be presented in tabular format i.e. numerically or graphically. In graphical form data are presented in differential and cumulative distribution curves (DSD and CUSD). Both the forms are interrelated, if one differentiated the cumulative distribution curve, the differential distribution is obtained. On the other hand, if one integrated the differential distribution curve, the cumulative distribution is obtained. The differential distribution shows the relative amount at each particle size. From the different size distribution, measures of central tendency such as the modal and mean diameters are determined. The diameter at the peak of the differential distribution is the modal diameter while the mean diameter is the average diameter.

The corresponding cumulative distribution curve demonstrates the relative amount at or below a particular size. The median diameter is another measure of central tendency. It is the diameter at the 50^{th} percentile, designed d_{50}. Quartile diameters include d_{75}, d_{50} and d_{25}. There are several measures of absolute width one can derive given the cumulative distribution. One common measure is the span, d_{90}-d_{10}. A dimensionless measure of width is the relative span defined as span/d_{50}. Other relative measures of width include percentile ratios such as d_{90}/d_{10} and d_{75}/d_{25}, which represents the spread across different segments of the distributions [7]. Previously, Modi et al reported the role of Mg^{2+} to change the particle shape from spherical to needle shape and on magnetic properties in the

system $Mg_xMn_{1-x}Fe_2O_4$ [8,9]. In the present work we aim to investigate influence of Mg^{2+} on particle size distribution for nanocrystalline spinel ferrite system $Mg_xMn_{1-x}Fe_2O_4$with the help of two representative compositions 0.2 and 0.4.

2. Experimental techniques

The spinel ferrite system $Mg_xMn_{1-x}Fe_2O_4$ with variable compositions x = 0.0, 0.1,0.2, 0.4 and 0.5 was prepared by air oxidation of an aqueous suspension containing Mg^{2+}, Mn^{2+} and Fe^{2+} cations in stoichiometric proportions. The starting solutions were prepared by mixing 50ml of aqueous solutions of $MgSO_4.7H_2O$, $MnSO_4.H_2O$ and $FeSO_4.7H_2O$ in proper proportions. A 2M solution of NaOH was prepared as a precipitant. The starting solution (pH ~ 3.5) was added into the precipitant because the solubility product constants for the hydroxides of the cation are exceeded [9] and sequential precipitation of the hydroxides can be avoided. The suspension (pH = 10.5) containing dark green intermediate precipitates was formed. Then the suspension was heated and kept at 60°Ctemperature, while hydrogen peroxide (H_2O_2) was added to promote oxidation reaction until all the intermediate precipitates changed into the dark brownish precipitates of the spinel ferrite (as prepared samples or precursor). The samples were filtered, washed by acetone and dried at 200°C under vacuum (final product). The preparation of ferrite powders by the oxidation method consists of oxidation by air(O_2) bubbling through an aqueous solution containing ferrous ions (Fe^{2+}) and other divalent ions (M^{2+}) after an alkaline solution (ROH) has been added, the reaction is given by: $Fe^{2+} + M^{2+} + ROH + O_2 \rightarrow M^{2+}{}_{1-x}Fe^{3+}{}_{2-x}O_4$where, ROH is NaOH, KOH, NH_4OH etc. Thus, ferrite powders of high homogeneity and purity are obtained [10]. The stoichiometry of the powdered samples was checked by energy dispersive analysis of X-rays (EDAX). X-ray diffraction data were collected on a Philips PW 1710 automated X-ray powder diffractometer using CuK_αradiation, graphite monochromator, and Xe-filled proportional counter. Micro structural characterization was performed by transmission electron microscopy (TEM), using a TECNAIK20 (Philips) microscope operated at 200 kV. For the TEM observations, the powder was first dispersed in amyl acetate by ultrasonication and then the suspension was dropped on a copper grid with a carbon film. Particle size distribution study has been carried out by Symantec Helos BF Range: 0.1 to 875 microns; 32 Multi element detector.

3. Results and discussion

The EDAX spectra displayed in Fig. 1 clearly demonstrate a group of three well defined peaks located between energy 5.5 keV to 7.0 keV. The maximum observed at ~ 6.4 keV is directly related to FeK_α, peak at ~ 7.0 keV corresponding to $FeK_{\beta1}$ and peak at~6.0 keV belongs to MnK_α characteristic line. It is important to note that MnK_β line interferes with FeK_α line in the spectra [11]. The peak located at ~ 1.254 keV confirms the present of MgK_α characteristic line. Here, care should be taken as MgK_β(1.3 keV) line overlaps with MgK_α line. The maximum on the left part of the spectra at ~ 0.5 keV clearly comes from OK_α, while very small peak that located at ~ 0.75 keV comes from $FeL_{\alpha1}$ characteristic line. The peak at extreme left of the spectra centered at ~ 0.25 keV connected with carbon (CK_α) characteristic line of impurity. The origin of sodium impurity is well understood from the chemical used for the synthesis of spinel ferrite system in which NaOH is used as a precipitant. On the other hand, impurity like carbon was likely to have been introduced from carbon coated shield to the pole pieces and special EDAX specimen holder made of carbon, beryllium and aluminum used in EDAX spectrometer [12]. It is well established fact that if a K_α line is identified in a spectrum, then a K_β line should exist. Furthermore, K_β line has intensity 1/10 of intensity of K_α line,i.e. K_α:K_β = 10: 1 [12]. In the present case, we have also observed this relationship for FeK_α and $FeK_{\beta1}$line in the spectra.

Shown in Fig. 2 are the room temperature (300 K) X-ray powder diffraction patterns for the x = 0.2, 0.4 and 0.5 compositions of $Mg_xMn_{1-x}Fe_2O_4$ spinel ferrite system. All the diffraction patterns were indexed and lattice constant value for each composition was determined using 'Powder-X' software. It is seen that the diffraction patterns could be indexed for face centered cubic (*fcc*) structure of space group O_7^h (Fd3m).

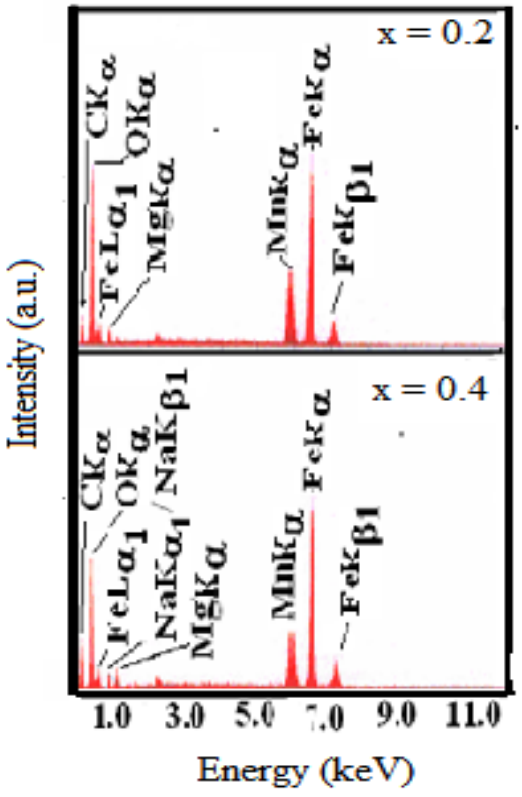

Fig. 1. EDAX spectra of x = 0.2 and 0.4 compositions of Mg-Mn ferrites (colour online)

No extra line corresponding to any other phase within the limit of X - ray detection which is typically 5 % or un-reacted ingredient was detected.

The cell edge parameter a (Å), for the different compositions of spinel ferrite system, $Mg_xMn_{1-x}Fe_2O_4$ has been determined with an accuracy of ± 0.002 Å and is given in Table 1.

Table 1. Lattice constant (a), X-ray density (ρ_x), bulk density (ρ), average particle size (D), surface area (S) and equivalent surface free energy (E_s) for nano crystalline Mg- Mn ferrites

x	a (Å) ±0.002Å	ρ_x (gm/cm^3)	ρ	P (%)	D (nm) ± 1 nm	S (m^2/gm)	E_s (cal/gm)
0.0	8.479	5.21	4.37	16.3	38	34.36	8.14
0.2	8.448	4.95	4.08	17.5	33	40.83	9.68
0.4	8.427	4.85	3.90	19.5	28	49.58	11.75
0.5	8.408	4.81	3.79	21.3	25	58.66	13.90

The lattice constant gradually decreases with increasing Mg^{2+}-concentration (x) (Table 1). This is due to the replacement of larger Mn^{2+} ion (0.83 Å) by smaller Mg^{2+} with ionic radius of 0.66 Å in the system. The lattice constant values for nano crystalline ferrite compositions under investigation are found smaller as compared to the ferrite ceramics of the same composition synthesized by the conventional double sintering ceramic technique, e.g. $MnFe_2O_4$(x = 0.0, a (Å) = 8.51 Å) [13]. This could be due to the one or more of the following reasons.

- Low degree of crystallinity in nanocrystalline ferrite materials [14].
- The change in the cation distribution taking place with different preparative parameters [10].
- The presence of lattice defects and its influence on the nano-particles, especially on the surface. In nanoparticles, surface energy and surface tension of the particles are high. This results in a tendency to shrink the lattice, which causes reduction in lattice constant [15].

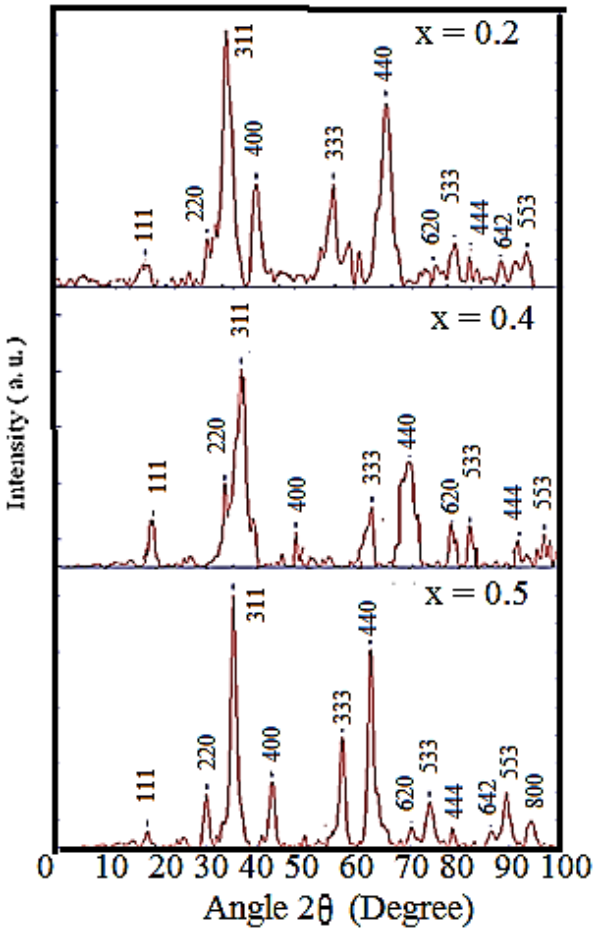

Fig. 2. X-ray powder diffraction patterns for Mg-Mn spinel ferrite materials recorded at 300 K (colour online)

The X-ray density for each composition was calculated, using the relation [20]: $\rho_x = ZM/N_A a^3$; where Z is the number of molecules per unit cell of the spinel lattice (Z=8), M is the molecular weight of the ferrite composition, N_A is the Avogadro's number and 'a' is the lattice constant. The lattice constant 'a' is found to decrease with *x*, thus, one can expect ρ_x to increase with *x*, but ρ_x is found to decrease with increasing magnesium content (*x*) in the system. This is due to the fact that rate of decrease of 'M' is faster than the rate of decrease of unit cell volume (a^3). In order to determine the bulk density (ρ) of each specimen in pellet form, precise value of weight measured by electronic balance and the volume measured by using travelling microscope. The ρ_x and ρ decrease with increase in Mg-content (*x*) i.e. the bulk density nearly reflects the same behavior of the theoretical density (Table 1). The porosity (P) of the samples was calculated using the values of X-ray density (ρ_x) and bulk density (ρ) by the relation; P= (f x 100 %), where, pore fraction (f) is given by the relation, $f = (1-\rho/\rho_x)$. The porosity values for the different compositions are given in Table1.

Apart from the phase identification and structural parameters determination, X-ray diffractogram can also be used for the determination of crystallite size from analysis of peak broadening. This can be understood by treating the crystal as a 3-dimensional grating. It is well known that a grating with larger number of slits gives narrower principal maxima. As the particle size is decreased, effectively the number of diffraction centers is reduced and the peak is broadened. The relationship between the broadening of diffraction peaks and the average crystallite size was derived by Scherrer and later it was modified by Bragg [16].The average particle size or thickness of the crystal grain diameter (D) for the different samples of Mg-Mn ferrite system with *x* = 0.0 – 0.5, was calculated from the broadening of the respective high intensity (311) peak using the Debye-Scherrer formula [16]: $D = K\lambda/B.\cos\theta$. Here, λ is the wave length of the CuK_α radiation (= 0.15418 nm), constant K (= 0.9) is related both to the crystallite shape and the way in which B and D are defined. B is the contribution to the XRD peak width due to the small size of crystallites in radians. The contribution must separate out from the measured line width B_M which includes instrumental broadening b, always parent irrespective of the particle size, for this one can record XRD pattern of a well crystallized, bulk standard material such as silicon powder under identical geometrical condition and measure the peak width b (= 0.08^o = 1.3955 x 10^{-3} Radian is taken). The broadening parameter B is obtained from the relation: $B= (B^2_M - b^2)^{1/2}$. The Scherrer formula is basically applicable to determine the diameter of spherical shaped nano particles (< 100 nm) only. The average particle diameter (D) calculated for *x* = 0.0, 0.2, 0.4 and 0.5 compositions are shown in Table 1. The particle size decreases from 38 nm for $MnFe_2O_4$ (*x* = 0.0) to 25 nm for $Mg_{0.5}Mn_{0.5}Fe_2O_4$ (*x* = 0.5) composition. It is clear by decreasing particle size that the number of atoms residing on the surface is increased.

In order to determine the cation distribution, X-ray diffraction line intensity calculations were made using the formula suggested by Buerger [17]:$I_{hkl} = |F_{hkl}|^2 P.L_p$; where I_{hkl} is the relative integrated intensity, F_{hkl} is the structure factor, P is the multiplicity factor(= $1+\cos^2\theta/\sin^2\theta\cos\theta$).

According to Ohnishi and Teranishi [18], the intensity ratios of planes I(220)/I(422) and I(400)/(422) are considered to be sensitive to the cation distribution parameter (*x*). There is a good contrast in the atomic scattering factor of Mg^{2+} and Mn^{2+}& Fe^{3+}cations present in the system. This makes the determination of the cation distribution quite reliable. Moreover, any alternation in the distribution of cation causes a significant change in the theoretical values of X-ray diffraction line intensity ratios. Therefore, in the process of arriving at the final cation distribution, the site occupancy of all the cations was varied for many combinations and those that agree with the experimental intensity ratios are shown in Table 2 [Ref.10].

Table 2. Cation distribution for $Mg_xMn_{1-x}Fe_2O_4$ system [Ref.10]

Composition	Cation distribution
$MnFe_2O_4$	$(Mn^{+2}_{0.52}\ Fe^{+3}_{0.48})^A\ [Mn^{2+}_{0.38}Fe^{+3}_{1.62}]^B\ O_4^{-2}$
$Mg_{0.2}Mn_{0.8}Fe_2O_4$	$(Mg^{+2}_{0.09}\ Mn^{+2}_{0.37}\ Fe^{+3}_{0.54})^A[Mg^{+2}_{0.11}\ Mn^{+2}_{0.43}\ Fe^{+3}_{1.46}]^BO_4^{-2}$
$Mg_{0.4}Mn_{0.6}Fe_2O_4$	$(Mg^{+2}_{0.25}\ Mn^{+2}_{0.13}\ Fe^{+3}_{0.62})^A[Mg^{+2}_{0.15}\ Mn^{+2}_{0.47}\ Fe^{+3}_{1.38}]^BO_4^{-2}$
$Mg_{0.5}Mn_{0.5}Fe_2O_4$	$(Mg^{+2}_{0.35}\ Fe^{+3}_{0.65})^A[Mg^{+2}_{0.15}Mn^{+2}_{0.50}\ Fe^{+3}_{1.35}]^BO_4^{-2}$

The grain morphology (shape, size and distribution) of nanocrystalline ferrite system under investigation were examined by transmission electron microscopy. Bright field TEM images (Fig. 3a and b) illustrate the nano scale nature of ferrite particles [14]. It can be seen that for *x* = 0.0 and 0.5 compositions, particles are quite well dispersed and not much agglomeration is present. The particles are perfectly spherical (Fig. 3(a)-(b)). The mean particle size for $MnFe_2O_4$ (*x* = 0.0) is found to be ~ 40 nm, which decreases with increasing Mg- concentration (*x*) and becomes ~ 27 nm for $Mg_{0.5}Mn_{0.5}Fe_2O_4$ (*x* = 0.5) composition. It is well known that materials with a cubic crystal structure are prone to grow into a spherical shape to minimize the surface tension [10,19]. Modi et al reported that substitution of Mg^{2+} in $MnFe_2O_4$ changes the shape of the particles gradually from spherical to lamellar to thick needle shape, which shows Mg^{2+} plays a vital role in particle's shape [8].

The observed decrease in particle size with increasing Mg^{2+} concentration (*x*) (*x* = 0.0 – 0.5) can be explained as follows. The crystal growth in the solution depends on various parameters, the most important being the molecular concentration of the material approaching the surface of the tiny crystal during the process of growth. Because of the liberation of the latent heat at the surface, the local temperature is normally higher than the solution

temperature. The surface temperature affects the local molecular concentration at the crystal surface and hence the crystal growth [20]. It seems that the formation of $Mg_{0.5}Mn_{0.5}Fe_2O_4$ (x = 0.5) is more exothermic as compared to the formation of $MnFe_2O_4$ (x = 0.0). The enthalpy of formation is (–340) KJ/mole for $MnFe_2O_4$ and (–590.7) KJ/mole for $MgFe_2O_4$ [21,22]. Thus, it is expected that if one introduces magnesium in the system more amount of heat will be liberated, which will increase the surface temperature of the growing crystal, resulting in decrease of the molecular concentration approaching at the crystal surface and hence hindering the crystal growth. The particle size estimated from TEM is shown in Table 3. From Table 3 it is quite clear that particle size determined from TEM is slightly greater than the particle size estimated from XRD using Schrrer's formula. This is because X-ray diffraction gives the information of crystalline region only and the contribution from the amorphous grain surface does not contribute. On the other hand, TEM gives the complete picture of the nanoparticles. Earlier we have made an attempt to calculate particle size from Mossbauer spectra for the system under investigation [9], it is shown in Table 3. By analyzing TEM, XRD and Mossbauer results [9] for particle size, one can have almost complete picture of the particle size, their distribution and morphology. From this discussion we can conclude that Mg^{2+} plays vital role in decreasing the particle size for the system under investigation apart from particle shape and also on magnetic properties [9].

Particle size growth may be monitored during operations such as granulation or crystallization. Determining the particle size of powders requiring mixing is common since materials with similar and narrower distributions are less prone to segregation [23]. In chemical growth techniques such as co-precipitation, which is used here growth arises from preliminary nucleation and growth via 'seed and grow' mechanism pursed by Ostwald ripening. For tinier particle systems, where the growth has been cramped some indigenous seeds persist in the colloid. For the larger particle systems, a considerable percentage of the seeds have been noticed in the ripening mechanism accelerate a more homogeneous distribution of particle size [8].

The phenomenon in which tiny particulates in solution dissolve and deposit on sizable particles in order to reach a more thermodynamically steady state wherein the surface to area ratio is minimized is known as Ostwald ripening. This happens to owe to fact that molecules on the surface of particles are energetically unsteady than those within. Therefore, the unstable surface molecules often go into solution shrinking the particle over time and increasing the number of free molecules in solution. When the solution is supersaturated with the molecules of the shrinking particles, the free molecules will redeposit on the larger particles. Thus, tiny particulates diminish in size before they vanish and the sizable particles grow even bigger. The shrinking and growing of particles will bring about a larger mean diameter of a particle size distribution [8].

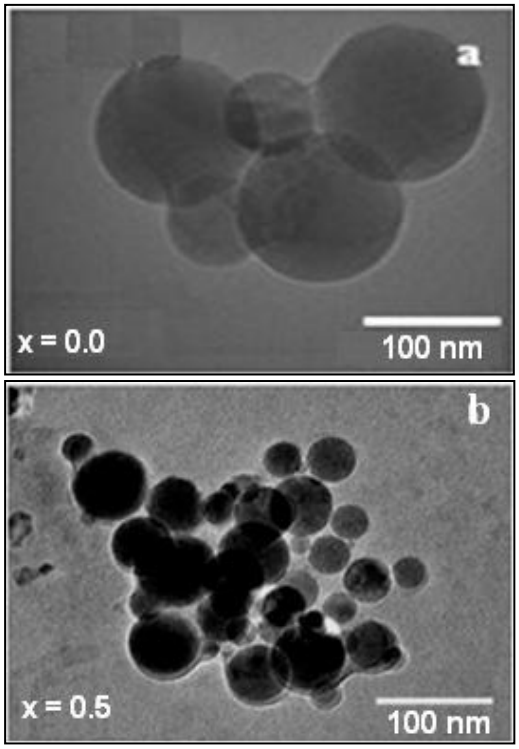

Fig. 3. TEM images for Mg-Mn ferrites. (a) and (b) – Spherical nano particles of $MnFe_2O_4$ (x = 0.0) and $Mn_{0.5}Mg_{0.5}Fe_2O_4$(x= 0.5) [Ref.10]

Table 3. Comparison of average particle size (D) for Mg-Mn ferrite from XRD, TEM and Mossbauer

Mg – content (x)	D (nm) [XRD] ±1nm	D (nm) [TEM] ±1nm	D (nm) Mossbauer [Ref. 9] ±1nm
0.0	38	40	42
0.2	33	36	33
0.4	28	31	30
0.5	25	27	22

The DSD and CUSD patterns for multiferroic spinel $Mg_xMn_{1-x}Fe_2O_4$ (x = 0.2, 0.4) are depicted in Fig. 5. Influence of Mg^{2+} on particle size distribution curves clearly reflected as it was in particle shape and size. Effect of Mg^{2+} substitution in the system reflected in DSD curve, this could be understood by various parameters derived from Fig. 5 and noted in Table 4. One can also understand influence of Mg^{2+} on particle size distribution through cation site preference of Mg^{2+}. From Table 2 it is quite clear that Mg^{2+} occupies tetrahedral or A – site and as the concentration of Mg^{2+} increases in A – site it is directly affect the particle size distribution curves for x = 0.2 and 0.4, on the other hand concentration of Mg^{2+} on the octahedral or B – site almost remains constant, so we can conclude that tetrahedral or A – site Mg^{2+} plays very important role in size distribution pattern. There are various measures of width. One of them is the full width at half maximum (FWHM). It is acquired by drawing a horizontal line at 50% of the maximum and taking the

difference between the two places, it intersects the distribution. The half width at half maximum (HWHM), is another measure of width and is described as FWHM/2. A relative fractional measure of width is derived by dividing HWHM by the measure of central tendency from which it was extracted, the model diameter (HWHM/modal diameter) [8].

The size of the particles shown in the Fig. 5 is in micrometer order. But these particles were agglomerates which were found to break further and further to sub micro level with more and more powerful ultrasonic de-agglomeration techniques. Particles, which are fundamentally of micron size cannot form sub-micron particles by ultrasonic treatments. Crystallites are small crystals to which a material, possibly, can be de-agglomerated if proper technique is available. So, the afore said crystallite size, 25-40 nm of Mg-Mn powders indicates that the fundamental size of this powder particles is of nano meter scale only and nano size particles can be formed from it if the powder could be efficiently de-agglomerated. Transmission electron micrograph (TEM) of these Mg-Mn ferrite powder samples supports this argument.

Table 4. Measurement of central tendency and width for Mg – Mn ferrites

Parameter	$x = 0.2$	$x = 0.4$
Modal diameter	50 μm	80 μm
Average diameter	70 μm	80 μm
FWHM	110 μm	92 μm
Span	95 μm	106 μm
Relative Span	2.11	2.35
Quartile ratio	6	10
Median diameter	45 μm	45 μm
Relative percent measure of width	78%	65%
$x = 0.2$: d_{10} = 5 μm, d_{25} = 10 μm, d_{50} = 45 μm, d_{75} = 60 μm, d_{90} = 100 μm $x = 0.4$: d_{10} = 4 μm, d_{25} = 8 μm, d_{50} = 45 μm, d_{75} = 80 μm, d_{90} = 110 μm		

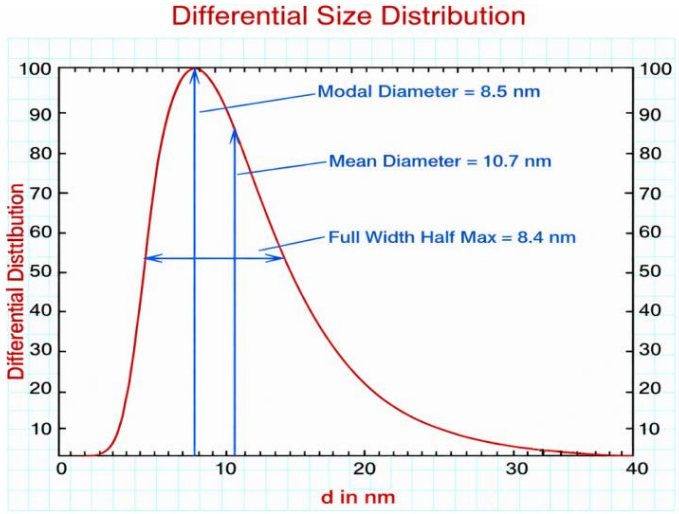

(a)

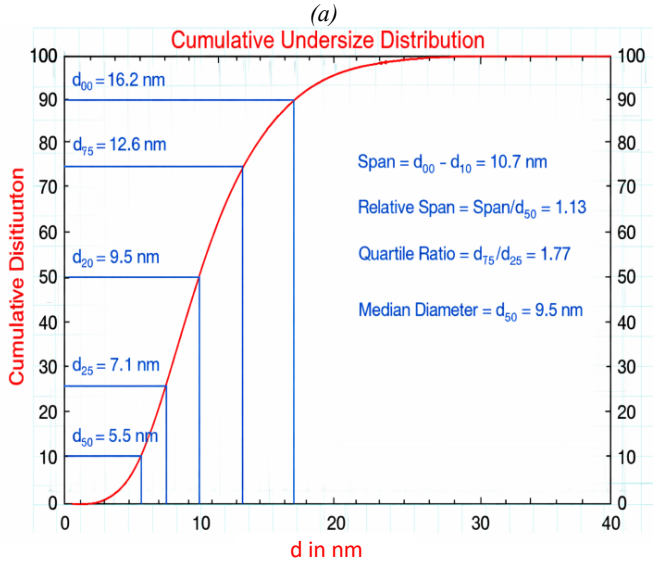

(b)

Fig. 4. Illustrative differential size distribution (a) and cumulative undersize distribution (b) curves [Ref.7] (colour online)

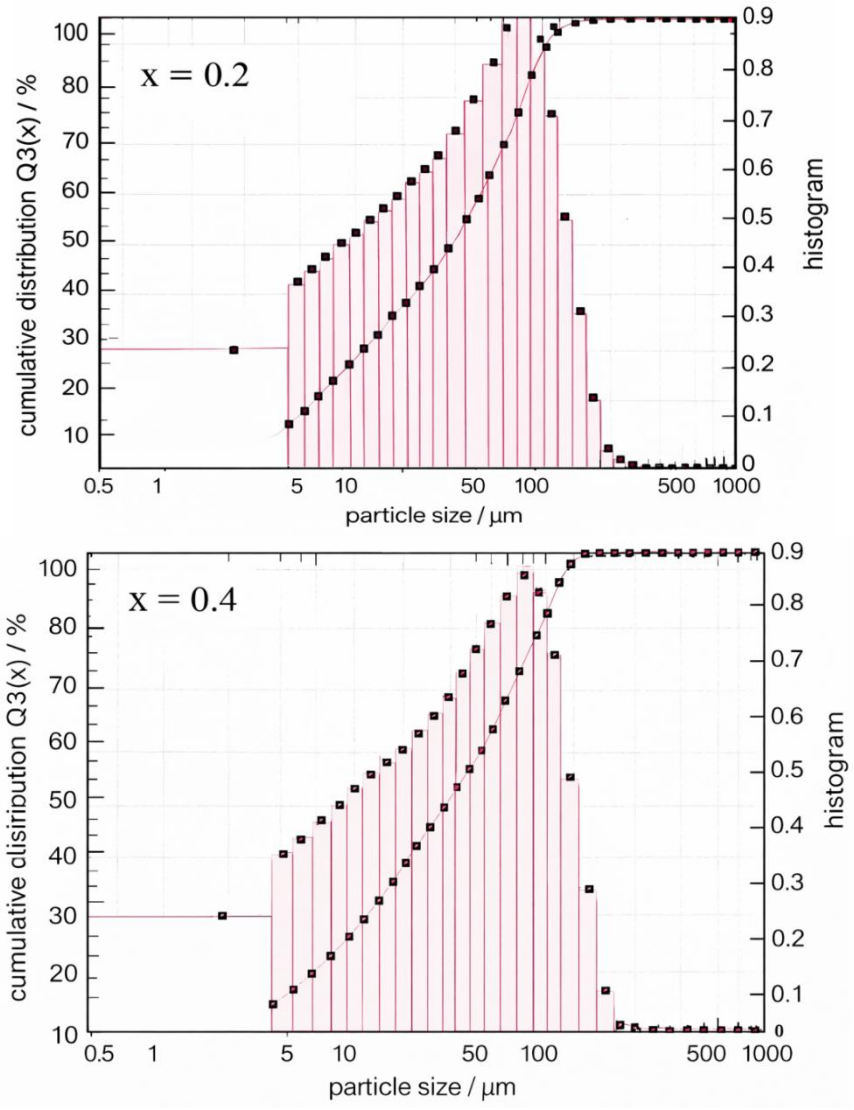

Fig. 5. Particle size distribution (DSD and CUSD curves) for x = 0.2 and 0.4composition

4. Conclusions

We have successfully synthesized nanocrystalline $Mg_xMn_{1-x}Fe_2O_4$, (x = 0.0 – 0.5) through coprecipitation method, stoichiometry of the samples was confirmed by EDAX and single phase as well as particle size determination by XRD technique respectively, broadening of the XRD peaks suggests particles with nano scale, further particle size reduces with substitution of Mg^{2+}, XRD, TEM and Mossbauer study supports these results.

The Particle size distribution curves analysis shows the influence of Mg^{2+}on particle size distribution in the composition. Influence of Mg^{2+} is also confirmed by various parameters derived for composition x = 0.2 and 0.4 (Table 4). The agreement between the particle size estimated with the help of Mossbauer, TEM and XRD pattern analysis can be regarded as quite satisfactory. Our previous study on effect of Mg^{2+} substitution on magnetic properties of same system also supports results and findings of this work. Furthermore, the distribution is unimodal, size of the particles is in micrometer order and ultrasonic deagglomeration is required before further analysis.

Acknowledgements

The authors are thankful to SICART (V. V. Nagar – Gujarat – India) for providing characterization facility.

References

[1] M. Popovici, C. Savii, D. Niznanskya, J. Subrt, J. Bohacek, D. Becherescu, C. Caizer, C. Enache, C. Ionescu, J. Optoelectron. Adv. M. **5**(1), 251 (2003).

[2] E. N. Lysenko, E. V. Nikolaev, V. A. Vlasov, A. S. Svirkov, A. P. Surzhikov, E. A. Sheveleva, I. V. Plotnikova, S. A. Artishchev, Russian Physics Journal **67**(7), 960 (2024).

[3] S. A. Bobuyok, A. P. Surzhikov, E. V. Nikolaev,

V. A. Vlasov, E. N. Lysenko, Russian Physics Journal **67**(5), 675 (2024).
[4] E. P. Naiden, Russian Physics Journal **50**(2), 170 (2007).
[5] E. P. Naiden, V. A. Zhuravlev, V. I. Itin, O. G. Terekhova, A. A. Magaeva, Yu. F. Ivanov, Russian Physics Journal **49**(9), 946 (2006).
[6] M. P. Bogdanovich, Russian Physics Journal **39**(10), 924 (1996).
[7] K. B. Modi, J. A. Bhalodia, T. K. Pathak, P. Y. Raval, P. R. Pansara, N. H. Vasoya, C. R. Kathad, S. J. Shah, International Journal of Scientific Research in Physics and Applied Sciences **6**(1), 29 (2018).
[8] Kunal B. Modi, Nimish H. Vasoya, Vinay K. Lakhani, Tushar K. Pathak, Journal of Advances in Microbiology Research **7**, 40 (2012).
[9] K. B. Modi, N. H. Vasoya, V. K. Lakhani, T. K. Pathak, Applied Nanoscience **5**, 11 (2015).
[10] T. K. Pathak, J. J. U. Buch, U. N. Trivedi, H. H. Joshi, K. B. Modi, Journal of Nanoscience and Nanotechnology **8**(8), 4181 (2008).
[11] http://www.charfac.umm.edu
[12] http://nanoanalysis.materials.ox.ac.uk
[13] Alex Goldman, Modern ferrite technology, 2nd edition, Springer, USA (2006).
[14] M. K. Rangolia, M. C. Chhantbar, A. R. Tanna, K. B. Modi, G. J. Baldha, H. H. Joshi, Indian Journal of Pure and Applied Physics **46**(1), 60 (2008).
[15] Z. J. Zhang, Z. L. Wang, B. C. Chakaumakos, J. S. Yin, Journal of the American Chemical Society **120**(8), 1800 (1998).
[16] B. D. Culity, Elements of X-ray diffraction, 2nd Edn., Addison Wesley Pub. Co., Reading, USA, 1978.
[17] M. J. Burger, Crystal Structure Analysis, John Wiley, New York, 1960.
[18] H. Ohinishi, T. Teranishi, Journal of the Physical Society of Japan **16**, 35 (1961).
[19] K. Parekh, R. V. Upadhyay, L. Belova, K. V. Rao, Nanotechnology **17**(24), 5970 (2006).
[20] Strickland Constable, Robert Frederick, Kinetics and mechanism of crystallization from the fluid phase and of the condensation and evaporation of liquids, Academic Press, 1968.
[21] B. S. Randhawa, M. Kaur, K. Gandotra, Journal of Radioanalytical and Nuclear Chemistry **269**(1), 69 (2006).
[22] B. S. Randhawa, M. Kaur, Journal of Radioanalytical and Nuclear Chemistry **261**(3), 569 (2004).
[23] http://www.Horiba.com.

*Corresponding author: tkpathak@gecrajkot.ac.in